

## **Supporting Information**

### **Sustainable one step process of making carbon-free TiO<sub>2</sub> anode and sodium-ion battery electrochemistry**

Tandeep S. Chadha<sup>a,#</sup>, Prasit Kumar Dutta<sup>b,#</sup>, Ramesh Raliya<sup>a</sup>, Sagar Mitra<sup>b,\*</sup>, Pratim Biswas<sup>a,\*</sup>

<sup>a</sup>Aerosol and Air Quality Research Laboratory, Department of Energy, Environmental and Chemical Engineering, Washington University in St. Louis, St. Louis, MO 63130, USA

<sup>b</sup>Electrochemical Energy Laboratory, Department of Energy Science and Engineering, Indian Institute of Technology Bombay, Mumbai - 400076, India

All the main evidences of the current study have been incorporated in the main manuscript while the supported scientific evidence have been included as supporting information.

## 1. Cycling Performance

It has been observed that the capacity improves significantly after slow rate initial cycling. After 200 cycles in case of normal cycling, 110 mAh g<sup>-1</sup> capacity was achieved (Figure S1) whereas the hysteresis provided 120 mAh g<sup>-1</sup> capacity after 1000 cycles while using the same current rate of 100 mA g<sup>-1</sup>(Figure 1b). In the initial 40 cycles, the capacity was low which may infer that this dendritic TiO<sub>2</sub> needs few initial cycles to build better electrode-electrolyte interface. In another way, this typical TiO<sub>2</sub> dendrites needs few initial cycles of electrochemical activation. Whereas, in the power cycling (Figure 1b), the rate was slow for initial cycles. Hence, such behaviour was not present there. Mass of the electrode for figure 1b and figure S1 were 0.16 mg and 0.116 mg.

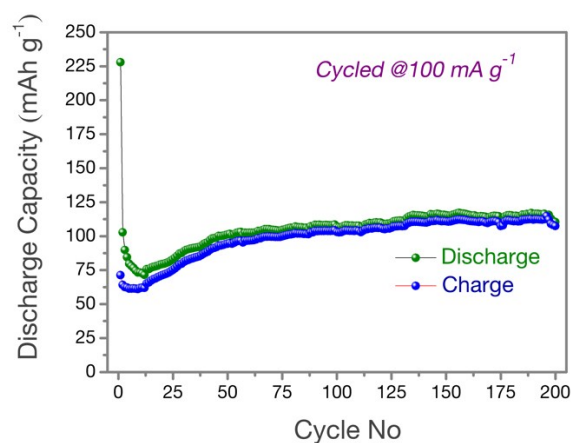


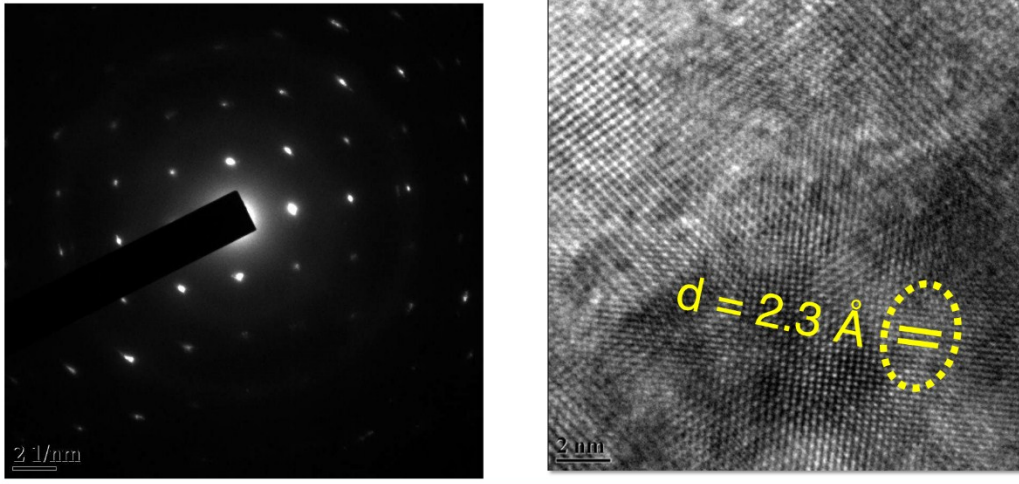
**Figure S1** Cycle life of anatase TiO<sub>2</sub> at 100 mA g<sup>-1</sup> current rate.

## 2. Change in Crystallography through TEM

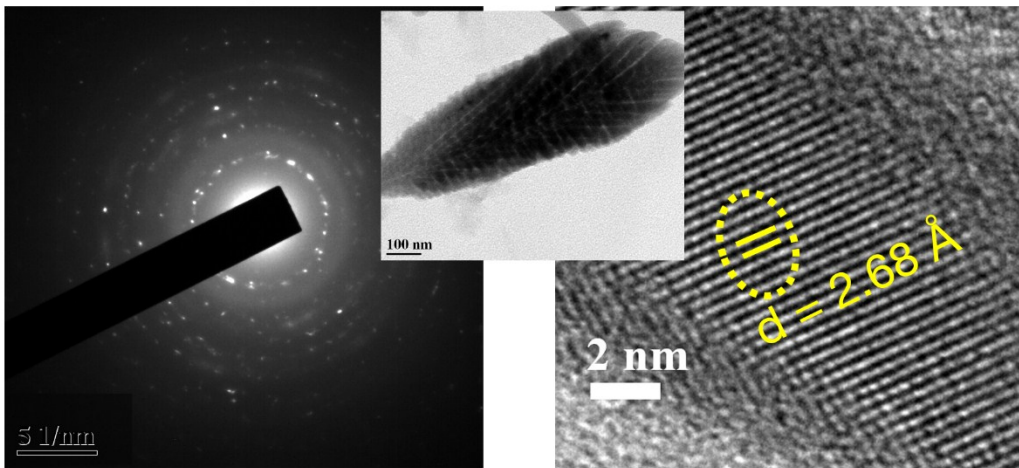
Here, we have compared three samples: as-prepared, after 500 cycles and after 1000 cycles (Figure S2). All samples were at de-sodiated state. Polycrystalline behavior has been explicitly

observed after cycling. The lattice spacing also increased upon cycling. This indicated cyclic stress to the lattice created by repeated sodium-ion insertion.

**a** Before Cycling



**b** After 500 Cycles



**c** After 1000 Cycles

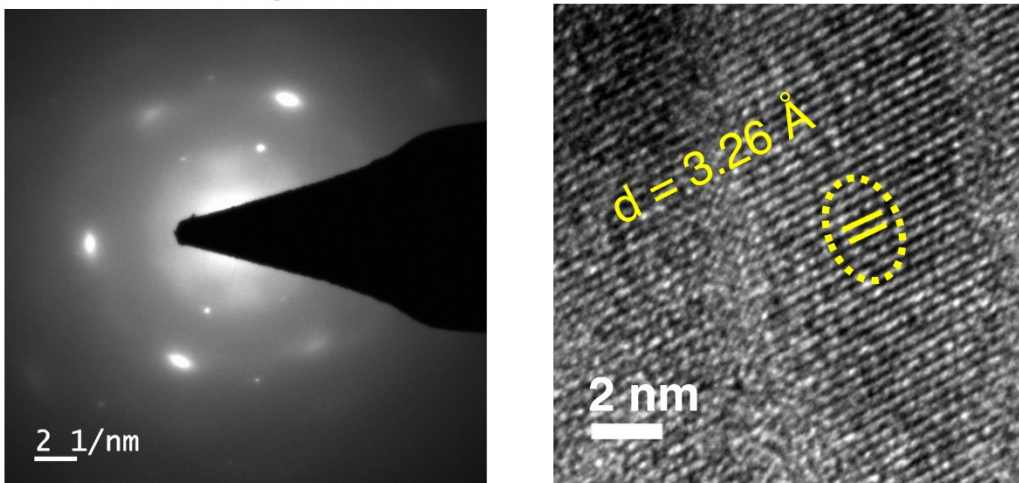


**Figure S2 (a-c)** TEM analysis of TiO<sub>2</sub> after 500 and 1000 cycles, compared with the initial stage.

### **3. Electrochemistry**

Charge-discharge performances at different current rates have been compared here (Figure S3, a). The corresponding dQ/dV plots were reflected the reaction position of the Na-ion insertion and de-insertion. Initially, the material need to activated electrochemically which has been reflected as an improvement in reversibility. Finally, the material affords more than 99.5% Coulombic efficiency (Table T1). In the initial cycles, an irreversible reaction has been observed near 0.2 V (Figure S3 b, specifically started below 0.4 V) which can be subjected to surface storage reaction. This peak disappears upon cycling and also, the Coulombic efficiency improves (Figure S3 c). The extra capacity was mainly due to non-faradic contribution in the initial cycles. According to the calculation, non-faradic capacities in the 2<sup>nd</sup>, 6<sup>th</sup>, 11<sup>th</sup>, 16<sup>th</sup>, and 21<sup>st</sup> cycle were 227, 94, 63, 48, 32 mAh g<sup>-1</sup> respectively.

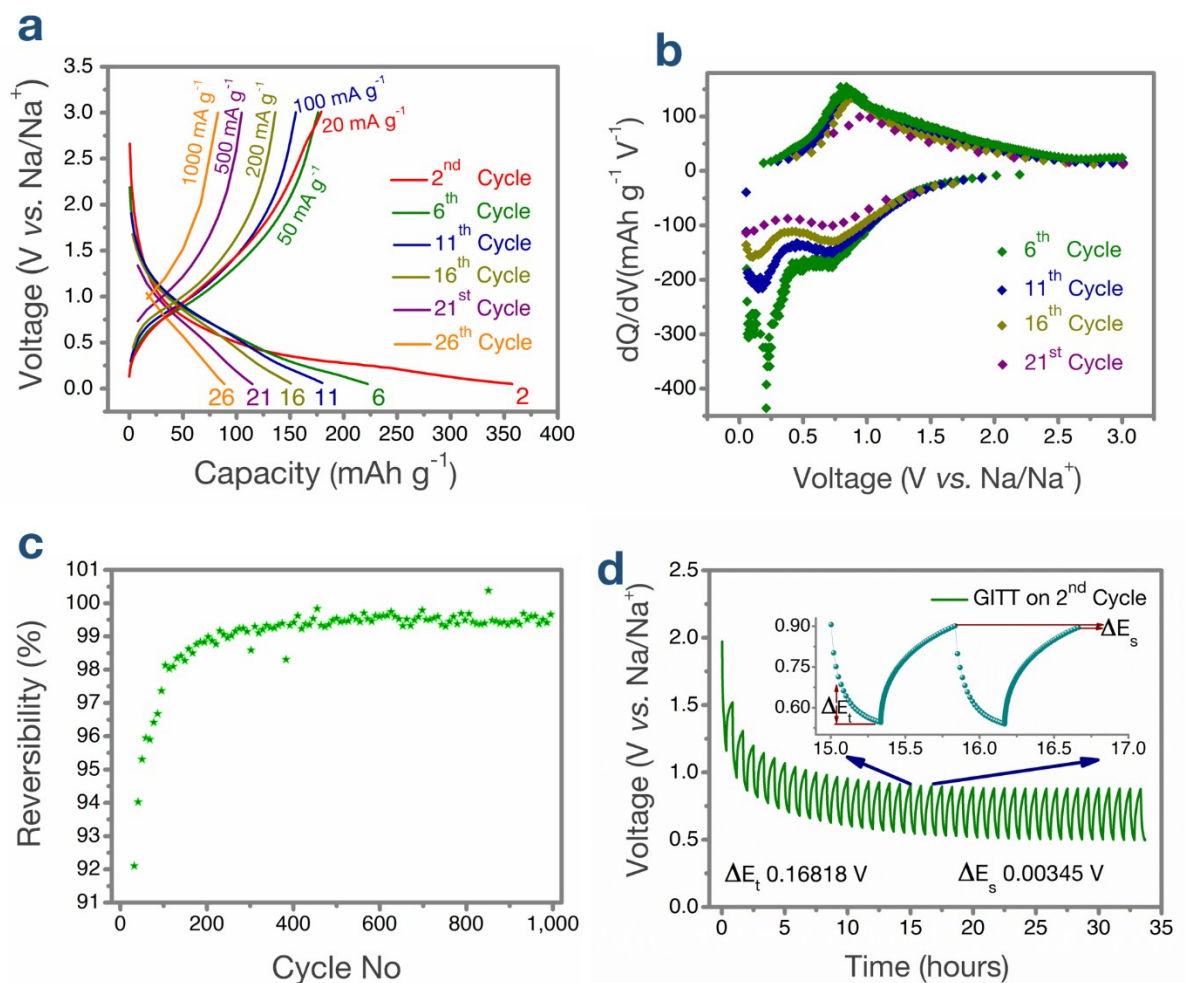


**Figure S3** (a) charge-discharge and (b)  $dQ/dV$  plots at power cycling; (c) reversibility at extended cycling and (d) GITT at 2<sup>nd</sup> cycle.

The Coulombic efficiencies at different cycles have been tabulated below to record the values of reversibility at different cycles.

**Table T1** Coulombic efficiencies at different cycles mentioned with different current rates.

Cycle No	Coulombic Efficiency (%)	Current Rate	Cycle No	Coulombic Efficiency (%)	Current Rate
2	50.26	20 mA g <sup>-1</sup>	50	95.31	100 mA g <sup>-1</sup>

<b>6</b>	79.22	50 mA g <sup>-1</sup>	<b>100</b>	97.62	100 mA g <sup>-1</sup>
<b>11</b>	86.59	100 mA g <sup>-1</sup>	<b>250</b>	99.08	100 mA g <sup>-1</sup>
<b>16</b>	90.14	200 mA g <sup>-1</sup>	<b>500</b>	99.58	100 mA g <sup>-1</sup>
<b>21</b>	91.28	500 mA g <sup>-1</sup>	<b>750</b>	99.47	100 mA g <sup>-1</sup>
<b>26</b>	92.65	1000 mA g <sup>-1</sup>	<b>1000</b>	99.55	100 mA g <sup>-1</sup>

The GITT experiment has been performed at the 2<sup>nd</sup> cycle (Figure S3 d) assuming that the 1<sup>st</sup> cycle involves few irreversible reactions. The diffusion co-efficient was calculated using the following equation<sup>[1]</sup>:

$$D = \frac{4 (n_m V_m)^2 \Delta E_s^2}{\pi \tau S^2 \Delta E_t^2}$$

where D is the diffusion co-efficient;  $\tau$  is the duration of the current pulse (s);  $n_m$  is the number of moles (mol);  $V_m$  is the molar volume of the electrode (cm<sup>3</sup> mol<sup>-1</sup>); S is the electrode/electrolyte contact area (cm<sup>2</sup>);  $\Delta E_s$  is the steady-state voltage change, due to the current pulse; and  $\Delta E_t$  is the voltage change during the constant current pulse, eliminating the  $iR$  drop.

In the case of the 2<sup>nd</sup> cycle (Fig. 2b), the calculation was done in the following manner:

$$\tau = 1200 \text{ sec}$$

$S = 11.14 \text{ cm}^2$  (calculated from the observed geometry and measured mass, assuming cylindrical columns)

$$n_m V_m = 4.87 \cdot 10^{-5} \text{ cm}^3$$

$$\Delta E_s = 0.00345 \text{ V}$$

$$\Delta E_t = 0.16818 \text{ V}$$

$$\text{Hence, } D = 8.53937 \times 10^{-18} \text{ cm}^2 \text{ s}^{-1}.$$

This calculation shows that the material is nearly 20 times higher than the previous report ( $\sim 4 \times 10^{-20} \text{ cm}^2 \text{ s}^{-1}$ ) in case of additive-free  $\text{TiO}_2$  anode for Na-ion battery.<sup>[2]</sup>

#### 4. Potentiostatic Electrochemical Impedance Spectroscopy

This *in-situ* experiment has been performed on the 1<sup>st</sup> discharge. We have measured the impedance from high frequency to low frequency at four different states-of-charges (WE vs. RE/CE potential), as depicted in Figure S4 a. At the last voltage point (0.05 V), the cell was disassembled, and FEG-SEM image was taken by tilting the columnar film. Wu *et al.* have observed flower-like features resulting from Na oxides formation after cycling<sup>[3]</sup>. Here, we observed no such changes in the surface morphology of the  $\text{TiO}_2$  columns after the first discharge (Figure S4 c), which might well explain the outstanding 1000 cycle electrochemical performance of these nanostructures.

Figure S4 a inset, shows the equivalent circuit, where  $R_e$  is indicative of the electrolyte resistance and associated uncompensated resistance arising from the instrumental components (corresponding to the high-frequency region),  $R_{SF}$  is the resistance due to surface film formation (corresponds to Na-metal electrolyte interface),  $R_{ct}$  is the charge transfer resistance ( $R_{SF}$  and  $R_{ct}$  are for medium-frequency region), and  $W$  (the Warburg impedance for low-frequency region) represents the diffusion of Na-ions into the solid  $\text{TiO}_2$  matrix<sup>[4]</sup>. In this typical case, curve fittings have been performed for the semi-circular regions. At OCV (without any current pulse), a small semi-circle is observed due to the presence of electrolyte-Na metal interface.<sup>[5]</sup> At 0.8 V, there are two semi-circles, one much larger than the other. The larger semi-circle is attributed to the formation of the SEI layer due to minimal decomposition of carbonates on the surface of the active material.<sup>[6]</sup>

The  $R_e$  shifted from 6.77 ohms to 13.35 ohms (avg.) and became constant at that value, indicating that an additional and stable uncompensated resistance was offered by the electrolyte as well as the SEI layer throughout the cycling. This stable resistance contributed to the exceptional durability of the  $\text{TiO}_2$  host. The larger semi-circular region was due to the charge transfer impedance (transfer of Na ions from the electrolyte to the surface), suggesting the initiation of reversible Na storage. But there was no observable change in the diffusive component as the low-frequency part shows high angle (with real Z axis). From 0.45 V onwards, the  $R_e$  contribution is not distinguishable, because the  $R_{ct}$  overlaps with it. At 0.45 V, the charge-transfer resistance increases,<sup>[7]</sup> which suggests that the transfer of Na-ions from the electrolyte to the surface encounters resistance because Na-ions are already present on the surface. At the last investigation voltage point, a sudden change in the low-frequency range depicts the storage of Na-ions on the surface of the  $\text{TiO}_2$ , which also confirms that the peaks near 0.1-0.2 V were due to surface storage of Na (Figure S3 b). Hence, this PEIS study confirms that the electrolyte used was able to create a stable SEI, enabling an easy transfer of Na ions into the host  $\text{TiO}_2$ .

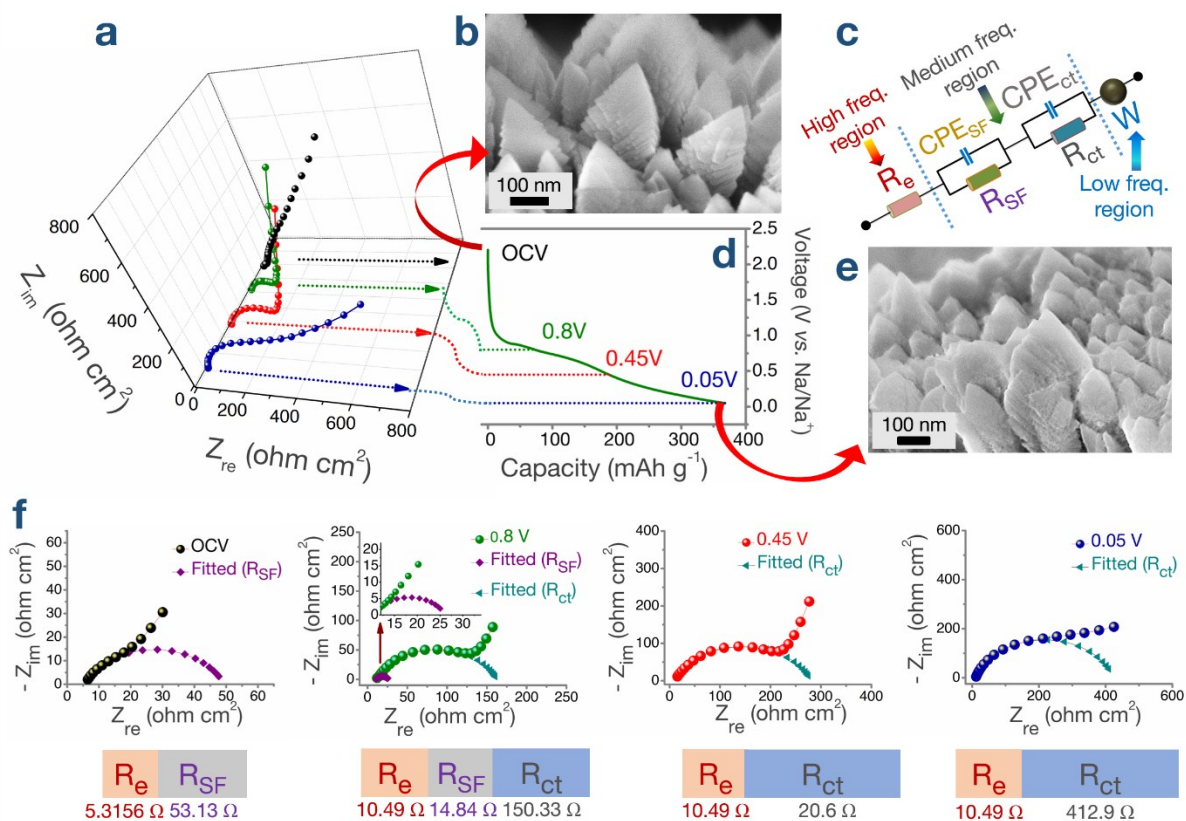


**Figure S4** (a) PEIS and data (d) analysis on 1<sup>st</sup> discharge cycles; inset: circuit for analysis and the SEM images (b) before and (c) after cycling.

## 5. Phase and Structural Changes upon Cycling

Initially, the pristine 1D grown (along (1 1 2) direction) TiO<sub>2</sub> changes crystalline structure by increasing the lattice parameters ( $a$  and  $c$ ). Hence, after sodiation, a strain-induced phase exists. After de-sodiation, the strain gets released from the lattice and anatase TiO<sub>2</sub> develops another co-existing rutile phase. This phenomenon has been depicted as  $E_g$  band in Raman spectra for de-sodiated samples (Figure S5 a, b) and as (1 1 0) plane in XRD (Figure S5 c) Also, the Figure S5 c has been cropped and incorporated as an inset in Figure 3 d. In the case of Raman spectra (Figure S5 b), surface means the beam was focused on the electrode surface which corresponds to the tip of the TiO<sub>2</sub> columns. Also, the word bulk means the beam was focused ~100 nm deep from the tip. Hence, the spectrum came from the bulk area of the columns.

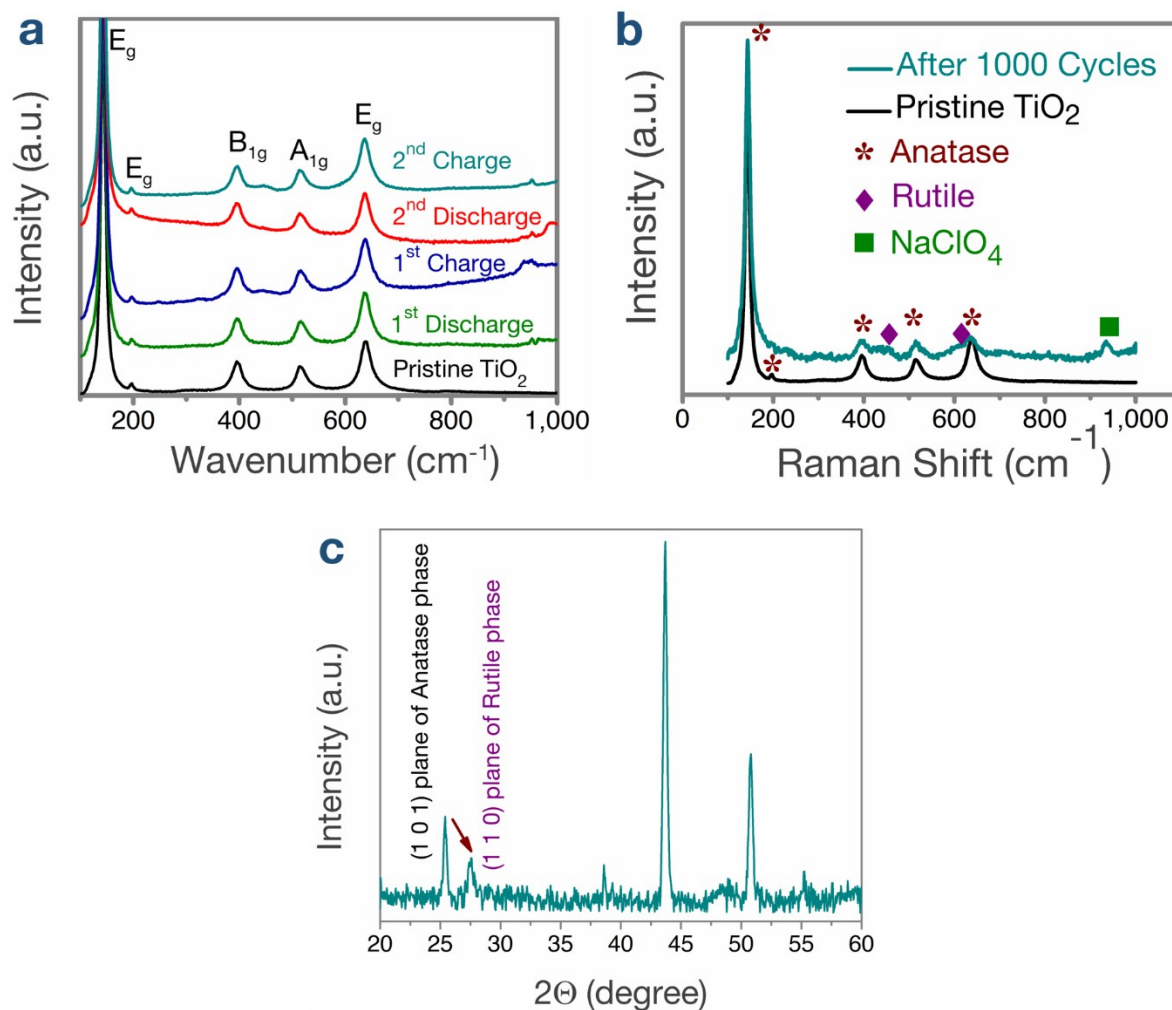


**Figure S5** (a) Raman spectra comparison among first 2 cycles, (b) after 1000 cycles and (c) X-ray diffraction pattern after 1000 cycles.

## 6. Importance of Water while Characterizing Cycled Samples for *ex-situ* TEM

Two different solvents were used to evaluate surface-stored Na and Na diffused inside the TiO<sub>2</sub> host. Cells were disassembled inside a glove box after cycling. The cycled electrode consisted of (i) diffused Na stored inside the solid TiO<sub>2</sub> medium, (ii) SEI and other trapped Na (possibly in some unknown form, such as metallic or semi-metallic clustered), and (iii) sticky electrolytes. The electrode was washed with PC (the solvent used for making the electrolyte), which helped to dissolve the salt NaClO<sub>4</sub> (as an electrolytic component) present onto the surface. This process made sure that no residual electrolyte was present on the surface. In the

next step, the SEI and trapped Na were removed by washing the electrode with water, since water reacts vigorously with Na. In this report, TiO<sub>2</sub> columns were dispersed in water and used for STEM-EDS analysis. Following another path, after washing the TiO<sub>2</sub> electrode with PC, we dispersed it into IPA (isopropyl alcohol). Typically, IPA did not remove SEI and associated trapped Na onto the surface. Hence, we were able to clearly differentiate Na stored on the surface from solid state Na in TiO<sub>2</sub> (Figure S6).

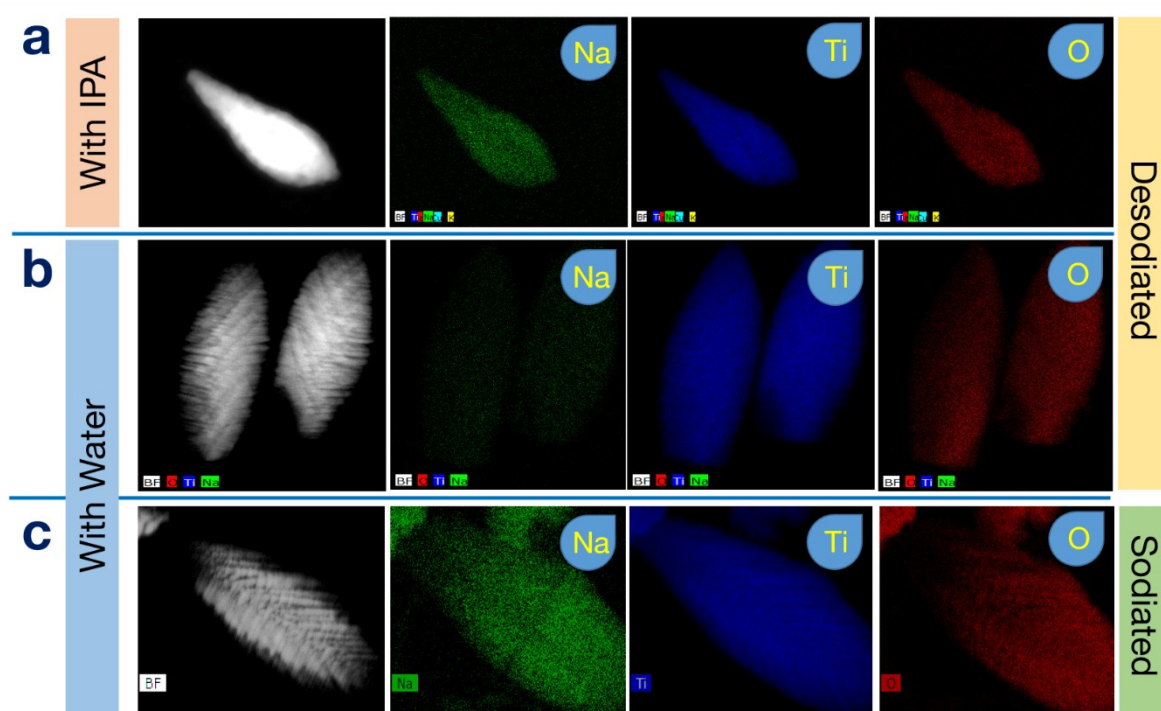


**Figure S6** Comparative *ex-situ* STEM-EDX images of de-sodiated TiO<sub>2</sub> columns washed with (a) IPA, (b) water and (c) sodiated TiO<sub>2</sub> columns washed with water.

## 7. Observation of Rotational Moiré Fringes

The HR-TEM images of the sodiated and de-sodiated sample during the first charge-discharge cycles are shown in Figure S7. The Figure S7 a has been used in Figure 4c in cropped form. Here, we are comparing the HR-TEM which explicitly show that sodiation has effect in lattice strain. After de-sodiation (Figure S7 b), the strain in lattice releases.

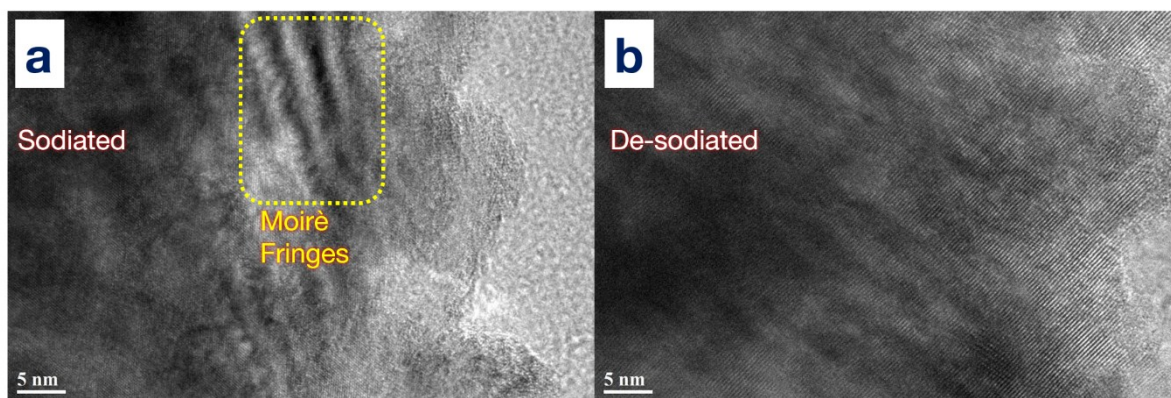


**Figure S7** HR-TEM images of the (a) sodiated and (b) de-sodiated TiO<sub>2</sub> columns.

### 7. Benchmarking of the Current Study

Here, we have benchmarked the current study with the reported literature which shows that the current study is in well-comparison with the existing literature. Nearly, 30% improvement in capacity is observed here.

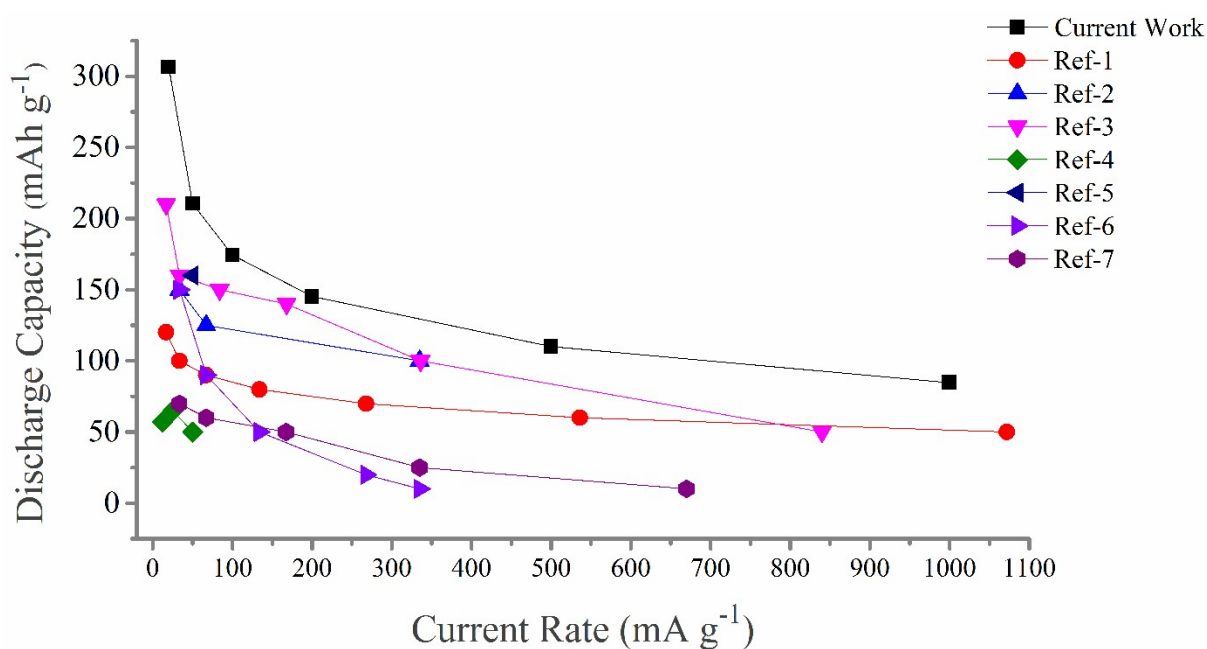


**Figure S8:** Benchmark curve for the current research in TiO<sub>2</sub> anode for SIB.

## Details of used references in Figure S8

Reference Number	Articles
Ref-1	H. Tao, M. Zhou, K. Wang, S. Cheng, K. Jiang, <i>Sci. Reports</i> <b>2017</b> , 7.
Ref-2	G. Longoni, R. L. Pena Cabrera, S. Polizzi, M. D'Arienzo, C. M. Mari, Y. Cui, R. Ruffo, <i>Nano Lett.</i> <b>2017</b> , 17, 992-1000.
Ref-3	H. He, D. Sun, Q. Zhang, F. Fu, Y. Tang, J. Guo, M. Shao, H. Wang, <i>ACS Appl. Mater Interfaces</i> <b>2017</b> , 9, 6093-6103.
Ref-4	D. Prutsch, M. Wilkening, I. Hanzu, <i>ACS Appl. Mater. Interfaces</i> <b>2015</b> , 7, 25757-25769.
Ref-5	H. Usui, S. Yoshioka, K. Wasada, M. Shimizu, H. Sakaguchi, <i>ACS Appl. Mater. Interfaces</i> <b>2015</b> , 7, 6567-6573.
Ref-6	H. Liu, K. Cao, X. Xu, L. Jiao, Y. Wang, H. Yuan, <i>ACS Appl. Mater. Interfaces</i> <b>2015</b> , 7, 11239-11245.
Ref-7	S. Qiu, L. Xiao, X. Ai, H. Yang, Y. Cao, <i>ACS Appl. Mater. Interfaces</i> <b>2016</b> , 9, 345-353.

## 8. Full Cell Study

We have studied the full cell behaviour with Prussian blue  $\text{Na}_{0.44}\text{Fe}^{\text{II}}\text{Fe}^{\text{III}}(\text{CN})_6$ . The cycle life and voltage profiles has been depicted in Figure S9b. The full cell produces an average of 2V. Capacity retention is nearly 80% over 30 cycles.

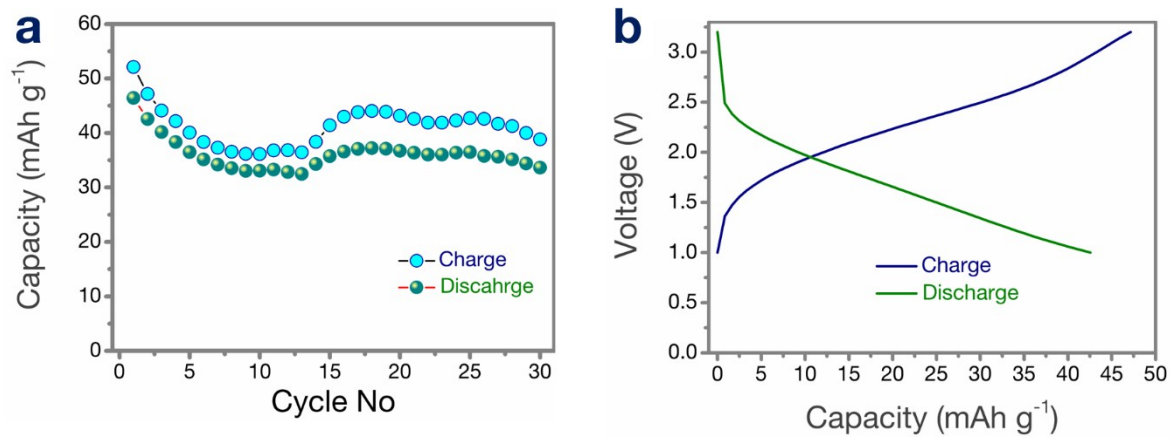


**Figure S9:** (a) Cycle life and (b) voltage profile of the TiO<sub>2</sub>-PB full cell.

## References

- [1] Z. Shen, L. Cao, C. D. Rahn, C.-Y. Wang, *J. Electrochem. Soc.* 2013, **160**, A1842.
- [2] D. Prutsch, M. Wilkening, I. Hanzu, *ACS Appl. Mater. Interfaces* 2015, **7**, 25757.
- [3] L. Wu, D. Bresser, D. Buchholz, G. A. Giffin, C. R. Castro, A. Ochel, S. Passerini, *Adv. Energy Mater.* 2015, **5**, 1401142.
- [4] D. Aurbach, *J. Power Sources* 2000, **89**, 206.
- [5] P. K. Dutta, S. Mitra, *J. Power Sources* 2017, **349**, 152.
- [6] A. Rudola, K. Saravanan, C. W. Mason, P. Balaya, *J Mater. Chem. A* 2013, **1**, 2653.
- [7] A. Langrock, Y. Xu, Y. Liu, S. Ehrman, A. Manivannan, C. Wang, *J. Power Sources* 2013, **223**, 62; D. Aurbach, A. Zaban, *J. Electroanal. Chem.* 1993, **348**, 155.